Multiferroicity of Non-Janus MXY (X=Se/S, Y=Te/Se) Monolayers with Giant In-Plane Ferroelectricity

Hafiz Ghulam Abbas,[a] Tekalign Terfa Debela,[b] Jae Ryang Hahn,[a,c] and Hong Seok Kang*[d]

[a]Department of Nanoscience and Technology, Research Institute of Physics and Chemistry, Jeonbuk National University, Jeonju 54896, Republic of Korea

[b]Institute for Application of Advanced Materials, Jeonju University, Chonju, Chonbuk 550 69, Republic of Korea

[c]Textile Engineering, Chemistry and Science, North Carolina State University 2401 Research Dr. Raleigh, NC 27695-8301, USA

[d]Department of Nano and Advanced Materials, College of Engineering, Jeonju University, Chonju, Chonbuk 55069, Republic of Korea

***Corresponding Author**: hsk@jj.ac.kr; jjhskang@gmail.com

Table S1. Various parameters of the different configurations of the MoSSe and WSSe monolayers in the 1H phase. Lattice parameters are the same for all the configurations. Corresponding data for the Janus configuration (S^1S^2) are also included.

	Config.	E_{rel}(meV)[a]	q[b]	∢(S-S),∢(S-Se), ∢(Se-Se)[c]	E_g(eV)[d]	Δ(meV)[e]	E_{CBM}(eV), E_{VBM}(eV)[f]
MoSSe	S^2Se^1	0.00	1.69, 1.70, -1.0, -1.0, -0.69, -0.70	3.23, 3.24, 3.23	1.49, 1.69	13, 174	(-3.97, -5.46), (-3.95, -5.64) Y'→Y'
	S^2Se^2	7	1.70, 1.68, -0.98, -0.98, -0.72, -0.70	3.10, 3.23, 3.23	1.44, 1.63	19, 168	(-4.03, -5.47), (-4.01, -5.64) Y'→Y'
	S^1S^2	35	1.70, 1.70, -0.96, -0.96, -0.74, -0.75	3.25, 3.24, 3.25	1.53, 1.70	14, 169	(-4.34, -5.87), (-4.33, -6.03) K→K
WSSe	S^2Se^1	0.00	2.01, 2.01, -1.17, -1.17,-0.84, -0.83	3.24, 3.25, 3.24	1.42, 1.82	34, 449	(-3.68,-5.10), (-3.65, -5.47) Y'→Y' Γ→Y'
	S^2Se^2	6	1.97, 1.97, -1.14, -1.14,-0.83, -0.83	3.12, 3.23, 3.23	1.35, 1.86	96, 436	(-3.75, -5.10), (-3.66, -5.52) Y'→Y' Γ→Y'
	S^1S^2	37	2.01, 2.01, -1.13, -1.14, -0.87, -0.88	3.23, 3.26, 3.23	1.45, 1.84	33, 440	(-4.03, -5.48), (-3.96, -5.80) K→Q Γ→K

[a]Relative energy per MSSe (M = Mo or W) with respect to the most stable configuration obtained from PBE-D3 calculations, respectively.

[b]The Bader charges of M^1, M^2, S^1, S^2, Se^1, and Se^2 atoms in sequence. See Figure 1, where S and Se in the MSSe correspond to Se and Te atoms in the MSeTe, respectively.

[c]The shortest bond distance between S-S, S-Se, and Se-Se in sequence

[d]Band gaps obtained from the PBE+SOC calculations for minority and majority spin components.

[e]The spin-orbit splitting at the CBM and VBM in the sequence obtained from the PBE+SOC calculations.

[f]The positions of the CBM and VBM in the sequence. Two parentheses are used to represent apparent positions for minority and majority spin components obtained from the PBE+SOC calculations in sequence.

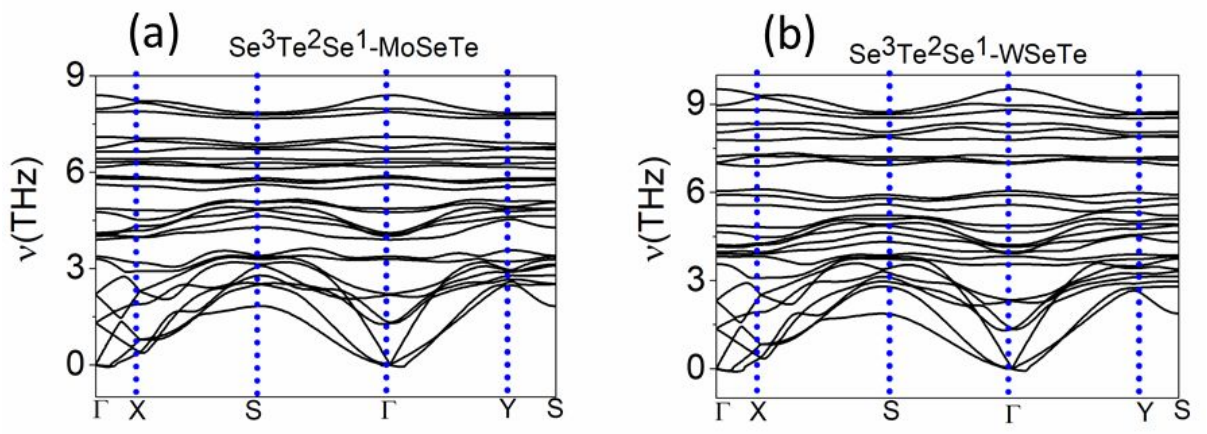

Figure S1. Phonon dispersion relations of (a) MoSeTe and (b) WSeTe MLs for $Se^3Te^2Se^1$ configuration.

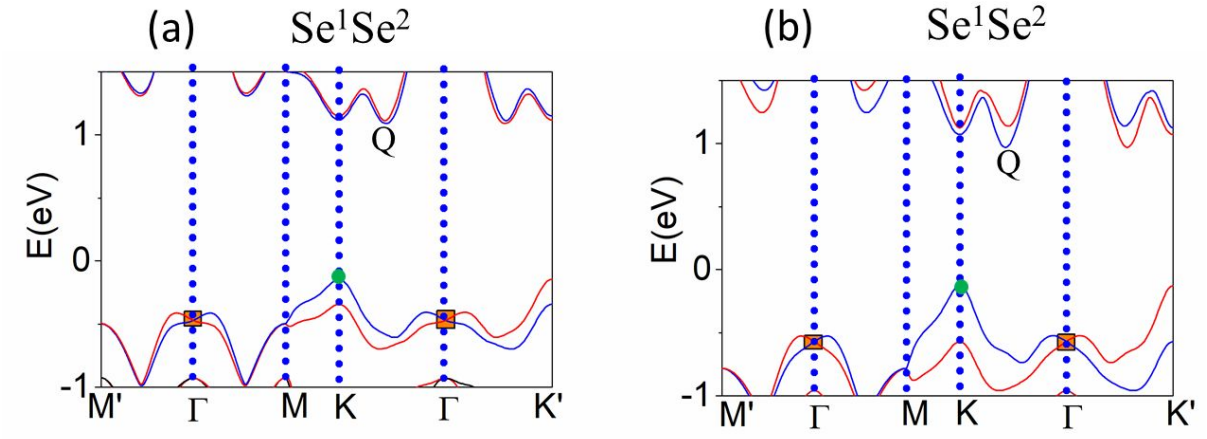

Figure S2. The PBE+SOC band structures of (a) MoSeTe and (b) WSeTe MLs for Janus (Se^1Se^2) configuration. Majority and minority spin channels are drawn by different colors, respectively.

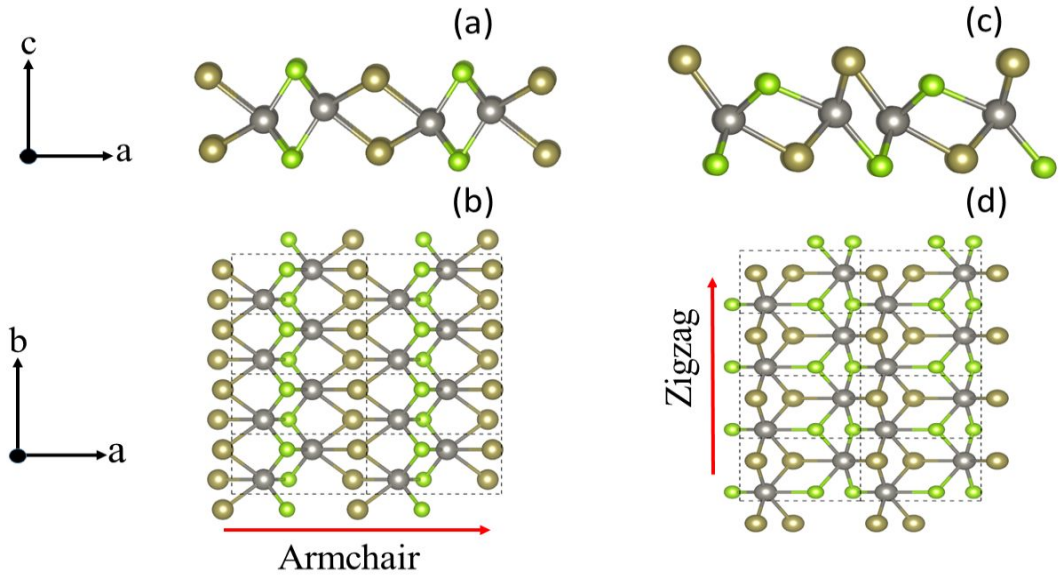

Figure S3. Chemical structures of the transition state (TS) for the FEC transition between $Se^2Te^2 \leftrightarrow (Se^2Te^2)^M$ mirror images with respect to the YZ plane under 15% uniaxial tensile strain along either armchair (//*a,* X) or zigzag (//*b,* Y) direction. Top (a and c) and side (b and d) views are shown. Grey, silver-white, and green balls represent W, Te, and Se atoms, respectively.

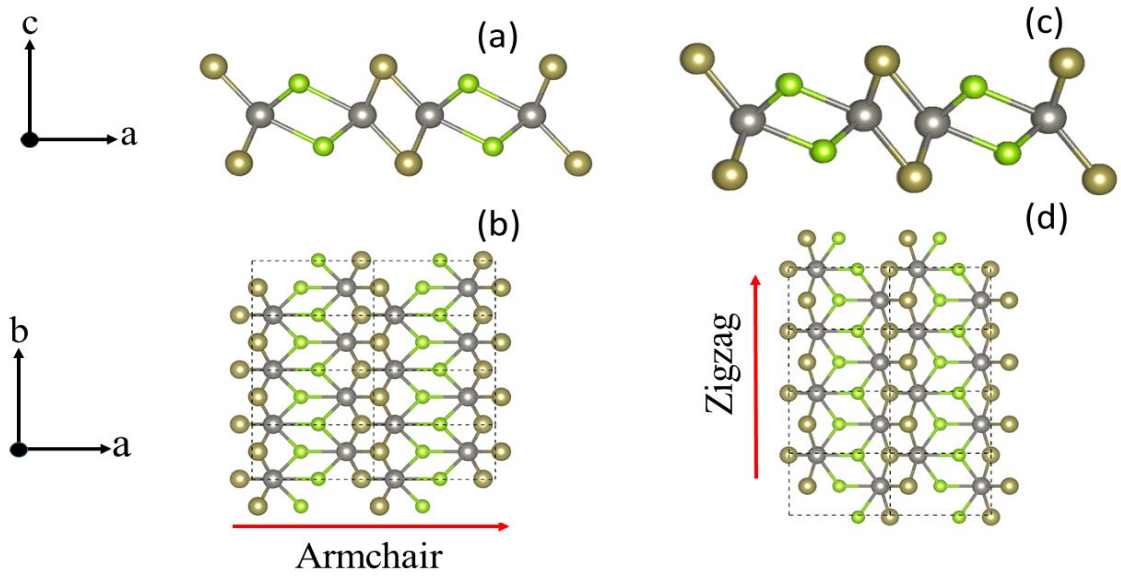

Figure S4. Chemical structures of the transition state (TS) for the FEL transition between $Se^2Te^1 \leftrightarrow Se^2Te^2$ under 15% uniaxial tensile strain along either armchair (//*a,* X) or zigzag (//*b,* Y) direction. Top (a and c) and side (b and d) views are shown. Grey, silver-white, and green

balls represent W, Te, and Se atoms, respectively